Clinical and Translational Radiation Oncology 39 (2023) 100582

Contents lists available at ScienceDirect

Clinical and Translational Radiation Oncology

journal homepage: www.sciencedirect.com/journal/clinical-and-translational-radiation-oncology

Original Research Article

Empirical planning target volume modeling for high precision MRI guided intracranial radiotherapy

James Stewart [a], Arjun Sahgal [a,b], Mahtab M. Zadeh [e], Bahareh Moazen [e], Pejman Jabehdar Maralani [d], Stephen Breen [b,c], Angus Lau [e], Shawn Binda [a], Brian Keller [b,c], Zain Husain [a,b], Sten Myrehaug [a,b], Jay Detsky [a,b], Hany Soliman [a,b], Chia-Lin Tseng [a,b], Mark Ruschin [b,c,e,*]

[a] Department of Radiation Oncology, Sunnybrook Odette Cancer Centre, Toronto, Canada
[b] Department of Radiation Oncology, University of Toronto, Toronto, Canada
[c] Department of Medical Physics, Sunnybrook Odette Cancer Centre, Toronto, Canada
[d] Department of Medical Imaging, University of Toronto, Sunnybrook Health Sciences Centre, Toronto, Canada
[e] Physical Sciences, Sunnybrook Research Institute, Toronto, Ontario, Canada

ARTICLE INFO

Keywords:
Intracranial Radiotherapy
PTV Margin
MRI guided Radiotherapy
Setup errors

ABSTRACT

Purpose: Magnetic resonance image-guided radiotherapy for intracranial indications is a promising advance; however, uncertainties remain for both target localization after translation-only MR setup and intrafraction motion. This investigation quantified these uncertainties and developed a population-based planning target volume (PTV) model to explore target and organ-at-risk (OAR) volumetric coverage tradeoffs.

Methods: Sixty-six patients, 49 with a primary brain tumor and 17 with a post-surgical resection cavity, treated on a 1.5T-based MR-linac across 1329 fractions were included. At each fraction, patients were setup by translation-only fusion of the online T1 MRI to the planning image. Each fusion was independently repeated offline accounting for rotations. The six degree-of-freedom difference between fusions was applied to transform the planning CTV at each fraction (CTV_{fx}). A PTV model parameterized by volumetric CTV_{fx} coverage, proportion of fractions, and proportion of patients was developed. Intrafraction motion was quantified in a 412 fraction subset as the fusion difference between post- and pre-irradiation T1 MRIs.

Results: For the left–right/anterior-posterior/superior-inferior axes, mean ± SD of the rotational fusion differences were 0.1 ± 0.8/0.1 ± 0.8/-0.2 ± 0.9°. Covering 98 % of the CTV_{fx} in 95 % of fractions in 95 % of patients required a 3 mm PTV margin. Margin reduction decreased PTV-OAR overlap; for example, the proportion of optic chiasm overlapped by the PTV was reduced up to 23.5 % by margin reduction from 4 mm to 3 mm.

Conclusions: An evidence-based PTV model was developed for brain cancer patients treated on the MR-linac. Informed by this model, we have clinically adopted a 3 mm PTV margin for conventionally fractionated intracranial patients.

Introduction

An emerging capability to improve the rigor and precision of radiotherapy delivery for treatment sites not fully visualized online with computed tomography (CT) based imaging is MR image-guided radiotherapy (MRIgRT) [1–3] due to its capacity to adapt directly to the soft tissue tumor volume. In the context of intracranial radiotherapy, such systems provide the ability to acquire T1 and T2 weighted images at each fraction to adapt the radiotherapy plan and accommodate target changes in high grade gliomas during conventionally fractionated intensity-modulated radiotherapy [4–7] and metastatic surgical cavities during hypofractionated stereotactic radiotherapy [8]. MRIgRT systems have the potential to maximize radiotherapy benefit for these dynamic changes, particularly in the setting of reduced clinical target volume (CTV) radiotherapy for gliomas [9,10] and surgical cavities [11–18].

The integration of MRI and linear accelerator technologies

* Corresponding author at: Department of Medical Physics, Odette Cancer Centre, Sunnybrook Health Sciences Centre, 2075 Bayview Avenue, Toronto, Ontario M4N 3M5, Canada.
E-mail address: mark.ruschin@sunnybrook.ca (M. Ruschin).

https://doi.org/10.1016/j.ctro.2023.100582
Received 11 January 2023; Accepted 12 January 2023
Available online 16 January 2023

introduces unique treatment challenges [3]. For example, the Elekta Unity MR-linac (MRL) employs a couch with an immovable position from the time of setup MR image acquisition through radiation delivery, and a fixed angle collimator. While a "virtual couch shift" or "adapt-to-position" strategy can accommodate translational patient setup errors under these constraints [1,19,20], rotational setup errors are not explicitly corrected unless the entire volume is re-contoured each fraction (termed "adapt-to-shape"). In order to apply an evidence-based planning target volume (PTV) for the treatment of intracranial tumors with the MRL, this investigation quantified rotational and motion uncertainties across a cohort of treated patient and produced a population-based PTV model. The model generates a parametric family of PTV margins and expedites exploration of the tradeoff between the competing clinical goals of target coverage and reducing normal brain tissue included in the PTV. Finally, in an extension of this model, the consequences of intrafraction motion were explored.

Methods and materials

Patient characteristics and treatment

Sixty-six patients with either a primary brain lesion (n = 49) or post-surgical metastatic resection cavity (n = 17) treated on the MRL across a total of 1,329 fractions were included. Patients from both indications were included in our analyses since, as will be detailed, both patient groups were setup and imaged with an identical protocol at both simulation and treatment. In addition, the combined group provides modeling data with a greater breadth in both CTV volumes and number of fractions per patient All patients were included from a prospective institutional research ethics board approved registry. General patient characteristics are summarized in Table 1.

All patients were imaged and treated as previously described [8,21]. In brief, both primary tumor and resection cavity patients were imaged prior to radiotherapy with a simulation computed tomography (CT) and simulation MR for planning purposes. The simulation CT was acquired on a Philips Brilliance Big Bore scanner with 0.88 × 0.88 × 1.00 mm voxels. A CT overlay, designed to mimic the couch top of the MRL, was placed on the couch of the CT scanner. An Orfit base plate (Orfit Industries NV, Belgium) was affixed to the overlay and a three-point mask used for patient immobilization. The simulation MR was performed on the 1.5 T Philips Ingenia MR scanner; T1c (T1 weighted sequence with Gadolinium contrast; 0.50 × 0.50 × 1.00 mm voxels) and T2-FLAIR (0.56 × 0.56 × 2.00 mm voxels) sequences were acquired. Contouring and radiotherapy planning were performed on the fused simulation images in the Monaco treatment planning system (Monaco v.5.40; Elekta AB, Stockholm, Sweden) with all contouring performed per consensus guidelines [22,23]. At each MRL fraction, the patient was again immobilized with a three-point mask attached to an Orfit base plate on the MRL couch. A non-contrast T1 MR sequence (0.50 × 0.50 × 1.00 mm voxels) was then acquired and fused to the simulation CT via a three degree-of-freedom translational-only image registration. This fusion was primarily based on matching to bony skull with an optional shift to account for soft tissue changes as identified by positional changes in organs-at-risk (OARs) such as the brainstem or optic chiasm per physician discretion. Fusion was performed to the planning CT, as opposed to the planning MRI, to enable plan optimization and dose computation per the adapt-to-position protocol [21]. Following this fusion, the online plan was then created based on the updated treatment isocentre using an adapt-to-position protocol [1,20]. In a subset of 412 fractions across 60 patients, a repeat non-contrast T1 MR sequence was acquired at end of fraction delivery for intrafraction motion quantification.

Primary intracranial tumors were treated with a median of 54 Gy (range: 40–60) in 30 (15–33) fractions using a 4 mm isotropic PTV margin. Due to occasional MRL unavailability due to service interruptions, some fractions were delivered on conventional linacs; a median of 28 (range: 13–32) fractions per patient were delivered on the MRL. Intracranial metastatic post-resection cavities were treated to either 27.5 or 30 Gy in 5 fractions, all of which were delivered on the MRL using a 2 mm PTV margin protocol.

Table 1
Patient Characteristics.

Characteristic	N = 66
Median Age (Range)	54.5 (21–82)
Sex	
Male	34 (52 %)
Female	32 (48 %)
Diagnosis	
Primary Intracranial	
Glioma	
Glioblastoma	27 (40.9 %)
Astrocytoma	11 (16.7 %)
Oligodendroglioma	4 (6.1 %)
Ependymoma	1 (1.5 %)
Unknown low-grade glioma	1 (1.5 %)
Meningioma	3 (4.5 %)
Pineal Tumor	1 (1.5 %)
Schwannoma	1 (1.5 %)
Metastatic Post-Resection Cavity	
Breast	6 (9.1 %)
Lung	6 (9.1 %)
Colorectal	2 (3.0 %)
Cervix	1 (1.5 %)
Endometrial	1 (1.5 %)
Renal	1 (1.5 %)
Radiotherapy Prescription Dose	Median (Range)
Primary Intracranial	54 (40–60) Gy
Metastatic Post-Resection Cavity	30 (27.5–30) Gy
Number of Fractions	
Primary Intracranial	15 (N = 12; 18.1 %)
	25 (N = 1; 1.5 %)
	30 (N = 35; 53.0 %)
	33 (N = 1; 1.5 %)
Metastatic Post-Resection Cavity	5 (N = 17; 25.8 %)

Target rotational uncertainty and intrafraction motion quantification

The non-contrast T1 MR images acquired at each treatment fraction were independently co-registered to the respective planning CT using a six degree-of-freedom translational and rotational match. This offline fusion was based solely on a bony skull match. These offline registrations were compared to the corresponding (translation only) online fusion with the target rotational uncertainty defined as the rotational component of the offline fusion. Note that the translational difference between the offline and online fusions are not representative of patient setup errors and are largely a byproduct of the image rotation point location. To avoid potential confusion, these translational components are not explicitly reported.

In the subset of patient fractions with repeat T1 MR imaging at end of radiation delivery, intrafraction motion was defined for both translational and rotational components as the difference between the end and start of treatment fusions. For example, if the left–right axis rotation was 1.5° and 1.0° for the end and start of treatment fusions, respectively, the intrafraction motion would be 0.5° for this axis. Thus, any non-zero translation or rotation in these data reflect intrafraction motion.

Planning target volume modeling

As illustrated in Fig. 1, a PTV (isotropic expansion of the planning CTV (CTV_{plan})) strategy can be conservative encompassing the misaligned fractional CTV (CTV_{fx}), or more balanced by reducing volumetric CTV_{fx} coverage at some fractions to reduce PTV overlap of nearby healthy tissue. To analyze and visualize this tradeoff, we developed a population-based model parameterized by the relative thresholds (CTV_{min}, Fx_{min}, Pt_{min}), which quantified the minimum PTV margin to

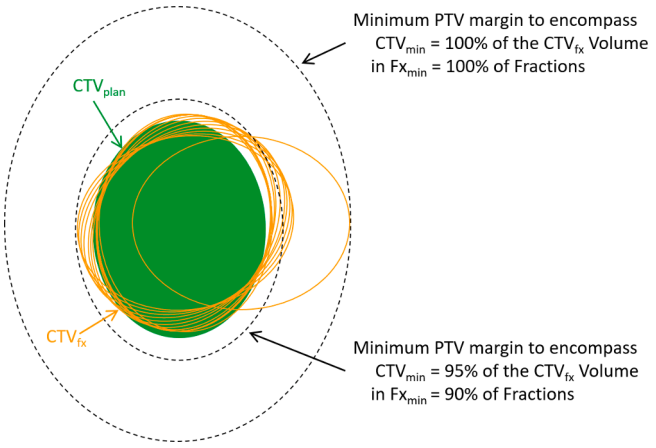

Fig. 1. Schematic ten fraction illustration of PTV margin modelling to accommodate target rotational and intrafraction motion uncertainties. Due to these uncertainties, the fractional CTVs (CTV_{fx}; orange ellipses) are misaligned relative to the planning CTV (CTV_{plan}; green ellipse); nine fractions with small rotational errors and one exaggerated outlier fraction are illustrated. The PTV margin model uses these empirically derived CTVs to generate a parametric family of margins, two such margins are delineated in the dashed black ellipses. (For interpretation of the references to colour in this figure legend, the reader is referred to the web version of this article.)

encompass CTV_{min} of the CTV_{fx} volume in $\geq Fx_{min}$ of fractions and in $\geq Pt_{min}$ of patients. As demonstrative examples, we use the model to determine the PTV margin for the following sets of criteria:

A. $(CTV_{min}, Fx_{min}, Pt_{min}) = (98\ \%, 95\ \%, 95\ \%)$
B. $(CTV_{min}, Fx_{min}, Pt_{min}) = (95\ \%, 90\ \%, 90\ \%)$

The PTV model was created using custom MATLAB scripts (MATLAB 2020a; The Mathworks Inc., Natick, Massachusetts). In brief, after exporting the planning contours for each patient from the Monaco planning system to DICOM RT structure sets, the CTV_{plan} contour was converted to a three-dimensional mask with 0.25 mm isotropic voxels. At each fraction, the translational and rotational difference between the offline and online fusions was converted to a transformation matrix and subsequently applied to the CTV_{plan} mask to generate a CTV_{fx} mask. The complete model was then generated by iterating over PTV_{min}, CTV_{min}, and Fx_{min} values, and at each iteration by counting the proportion of patients with $\geq Fx_{min}$ of their fractions containing $\geq CTV_{min}$ of the CTV_{fx} volume for the PTV margin PTV_{min}.

This baseline PTV model was extended for two specific problems. First, to model the effect of intrafraction motion, this model was applied to the 60 patient/412 fraction subset with post-fraction delivery repeat T1 imaging. Specifically, the model was generated with the rotational offsets from this subset, and also generated with this subset including intrafraction motion. Second, the sensitivity of PTV margins to residual rotational target localization uncertainties was analyzed by generating the model for different maximum rotational uncertainties. Denoting the maximum rotational uncertainty across the three patient axes at each patient fraction by $\max|\theta|$, the PTV model was generated for the subset of patient fractions that fell in the following categories:

1) $0.0^{\circ} \leq \max|\theta| \leq 0.5^{\circ}$, n = 362 of 1329 (27.2 %)
2) $0.5^{\circ} < \max|\theta| \leq 1.0^{\circ}$, n = 475 of 1329 (35.7 %)
3) $1.0^{\circ} < \max|\theta| \leq 1.5^{\circ}$, n = 259 of 1329 (19.5 %)
4) $1.5^{\circ} < \max|\theta|$, n = 233 of 1329 (17.5 %)

Modeling the PTV margin sensitivity to residual rotational setup uncertainties in this manner provides insight as to setting up rotational thresholds at the treatment unit for a given PTV.

Modelling benefits of PTV margin reduction

To quantify PTV overlap with healthy brain parenchyma and OARs, we modeled PTV margin reduction from 4 mm to 3 mm and to 2 mm. With our institutional protocol currently specifying a 2 mm PTV margin for 5-fraction hypofractionated radiosurgery surgical cavity patients, this approach is somewhat hypothetical for these patients but is still informative for other surgical cavity radiotherapy strategies in the community which employ larger PTV margins [24]. The PTV margin reduction modeling used methods similar to that from the previous subsection and the following metrics were quantified for both 3 and 2 mm margin PTVs relative to a 4 mm margin PTV:

1) The reduction in PTV volume.
2) The reduction in PTV overlap of healthy brain (brain excluding CTV_{plan}).
3) The reduction in PTV overlap of OARs (brainstem, optic chiasm, and optic nerves).

Results

Target rotational uncertainty and intrafraction motion quantification

Target rotational uncertainty measurements for all 1329 fractions are described in Fig. 2(a). The mean ± SD of this uncertainty along the left–right, anterior-posterios, and superior-inferior patient axes was 0.1 ± 0.8, 0.1 ± 0.8, and −0.2 ± 0.9°, respectively, with 84.4 % and 97.5 % of all rotations less than 1.0 and 2.0°, respectively.

Intrafraction motion measurements for the 60 patient/412 fraction subset are summarized in Fig. 2(b). Mean ± SD of the translational and rotational intrafraction motion was 0.0 ± 0.4, 0.1 ± 0.4, −0.1 ± 0.5 mm and −0.1 ± 0.6, 0.0 ± 0.5, 0.0 ± 0.4°, respectively. The magnitude of the translational intrafraction motion was less than 0.5 and 1.0 mm in 78.3 % and 94.8 % of all 3987 one-dimensional measurements, respectively. Similarly, the magnitude of the rotational intrafraction motion was less than 0.5 and 1.0° in 73.6 % and 93.5 % of measurements, respectively.

PTV modeling

The consequences of target rotational uncertainties on PTV margins are summarized in Fig. 3(a) which depicts the four dimensions of the PTV model by showing Fx_{min} values in the three plots, CTV_{min} values in the colored lines in each plot and PTV_{min} and Pt_{min} values along the x- and y-axis of the plots. The demonstrative examples are highlighted in Fig. 3(a). Specifically, PTV coverage of 98 % of the CTV_{fx} in 95 % of fractions in 95 % of patients (point A) required a 3.0 mm PTV margin. Similarly, coverage of 95 % of the CTV_{fx} in 90 % of fractions in 90 % of patients (point B) required a 1.5 mm margin. Rounding this PTV margin to 2.0 mm reveals that 95 % of the CTV_{fx} volume in 95 % of fractions in 94 % of patients would be covered by this 2.0 mm margin PTV.

The incorporation of intrafraction motion in the PTV model is shown in Fig. 3(b). The solid lines show PTV modeling of residual target rotational uncertainty for the 60 patient/412 fraction subset with intrafraction motion data. In other words, these solid lines show the results of the same model as Fig. 3(a), applied solely to the 412 (of 1329) fraction subset. After incorporating the intrafraction motion, the model was recomputed with the output shown in the dashed lines. Additional PTV margins of 0.5 and 0.2 mm are needed to accommodate intrafraction motion for scenarios A and B, respectively.

Modelling of PTV margin sensitivity to rotational target localization uncertainties is summarized in Fig. 4. Each of the four plots delineate the PTV model results for one of the four categories of maximum rotation ($\max|\theta|$) uncertainty for Fx_{min} = 95 %. For example, the top left plot shows the results for the 362 patient fraction subset with $\max|\theta| \leq 0.5^{\circ}$.

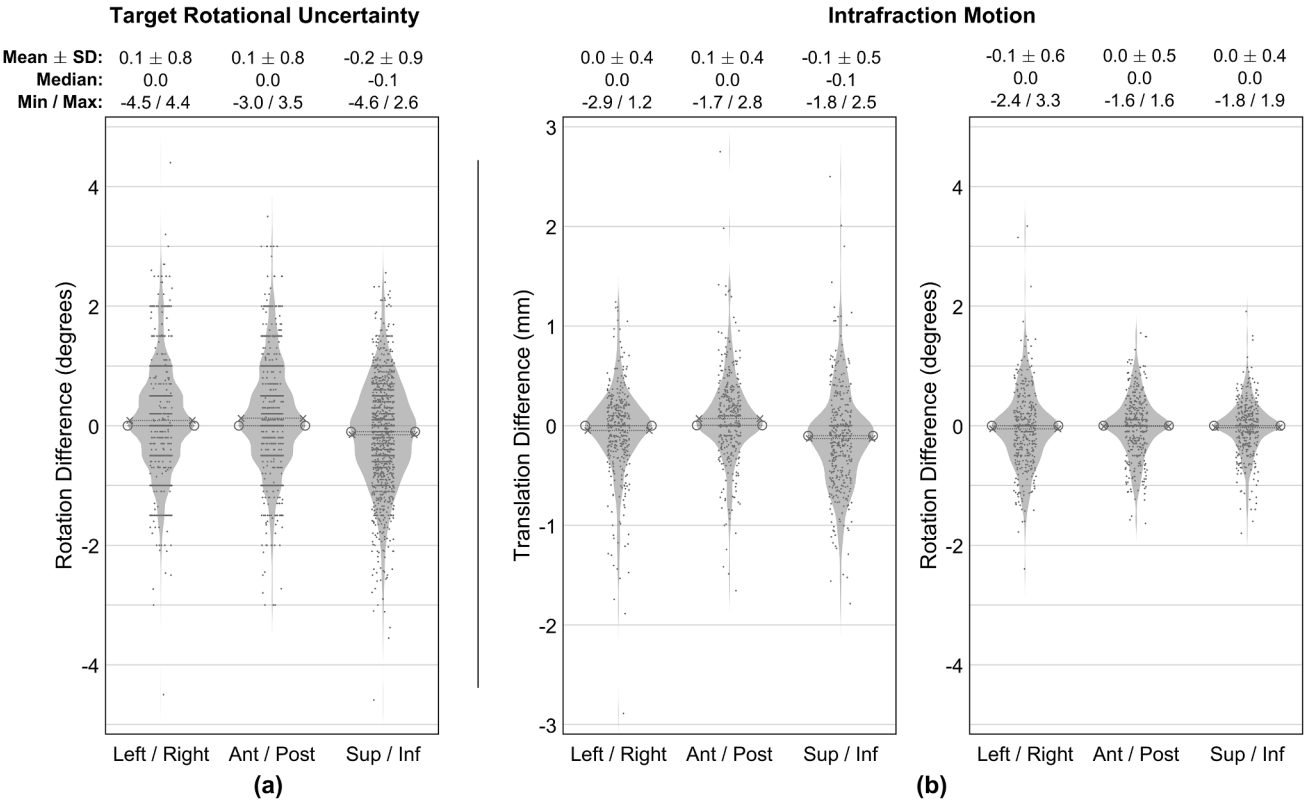

Fig. 2. Summary of target rotational uncertainties (a) and intrafraction motion (b). In (b), translational and rotational components are shown in the left and right plots, respectively. The violin plots in each subfigure delineate individual measurements (scatter points, randomly offset along the abscissa to improve visualization, n = 1329 and n = 412 in (a) and (b), respectively), probability density estimate (shaded region), mean (dashed line with 'x' endpoints), and median (dashed line with 'o' endpoints).

For reference, the faded lines in all plots delineate the results for all 1329 fractions; these are the same as the middle plot of Fig. 3(a). For the four categories of maximum rotation uncertainties, ($0.0^\circ \leq \max|\theta| \leq 0.5^\circ$, $0.5^\circ < \max|\theta| \leq 1.0^\circ$, $1.0^\circ < \max|\theta| \leq 1.5^\circ$, $1.5^\circ < \max|\theta|$), the modeled PTV margin was (1.9, 2.2, 2.1, 3.3) mm for scenario A and (1.0, 1.1, 1.0, 1.8) mm for scenario B.

Implications of PTV margin reduction

The modelled benefits of PTV margin reduction in terms of normal tissue sparing are outlined in Fig. 5. Relative to a 4 mm margin PTV, the volume of the PTV was reduced by a median of 8.9 % (range: 5.7–21.8 %) and 18.1 % (11.9–42.7 %) with a 3 and 2 mm PTV, respectively. This reduction was particularly pronounced in the n = 17 post-surgical cavity patients with a median PTV volume reductions of 17.2 % (range: 13.4–21.8 %) and 34.1 % (27.0–42.7 %) for 3 and 2 mm margin PTVs, respectively.

A total of 39 patients (59 %) had a 4 mm margin PTV that overlapped at least one OAR (brainstem, optic chiasm, or optic nerve). As outlined in Fig. 5, a decrease in this PTV margin substantially reduced the overlap of the PTV and these OAR, particularly in individual patients. For example, the 4 mm PTV of 32 patients (48 %) overlapped the optic chiasm. This volume of the optic chiasm overlapped by the PTV was reduced by up to 23.5 % and 35.9 % by decreasing the PTV margin to 3 and 2 mm, respectively.

Discussion

The intent of MRgRT is to improve confidence in irradiation accuracy for compact target volumes and to monitor and potentially adapt to clinically significant changes. A critical step to maximizing the clinical benefit of this technology is determining an evidence based PTV. In this investigation of intracranial tumors treated on the MR-linac with the adapt-to-position protocol, we determined that to ensure PTV coverage of 98 % of the CTV_{fx} volume in 95 % of fractions in 95 % of patients a PTV margin of 3.0 mm was required. For fractions with a maximum rotational setup uncertainty of 1.5°, this margin could be reduced to 2.2 mm under the same relative criteria. Informed by this model, we have clinically adopted a 3 mm PTV for conventionally fractionated intracranial patients and 2 mm for 5-fraction hypofractionated stereotactic radiosurgery patients on our MRL [8].

PTV margin recommendations are highly dependent on the specific radiotherapy platform and process, as noted in the original ICRU 50 PTV definition which states "(the PTV) size and shape depend primarily on the CTV, but also on the treatment technique used" [25]. In this respect, MRgRT platforms introduce challenging commissioning and quality assurance obstacles. Some of these challenges, such as gradient nonlinearity induced spatial distortion [26], susceptibility effects [27], and chemical shift artifacts [28] are inherent to MRI system. Others, however, result from the combination of MR imager and linear accelerator. These include, but are not limited to, the alignment of the imaging and treatment isocentres [29] and image quality variations at different gantry angles or during beam delivery [30]. Despite these difficulties, end-to-end irradiation targeting accuracy for unambiguous targets on the Elekta Unity MRL has been reported to be well under 1 mm [31]. Likely the largest uncertainty in intracranial radiotherapy, and one not limited to MRgRT platforms, is target delineation uncertainty. Although the addition of MR information to historic CT based contouring has reduced intracranial target contouring variability [32,33], target contouring inconsistencies still exist [34]. Recent comprehensive consensus contouring guidelines for MR-based

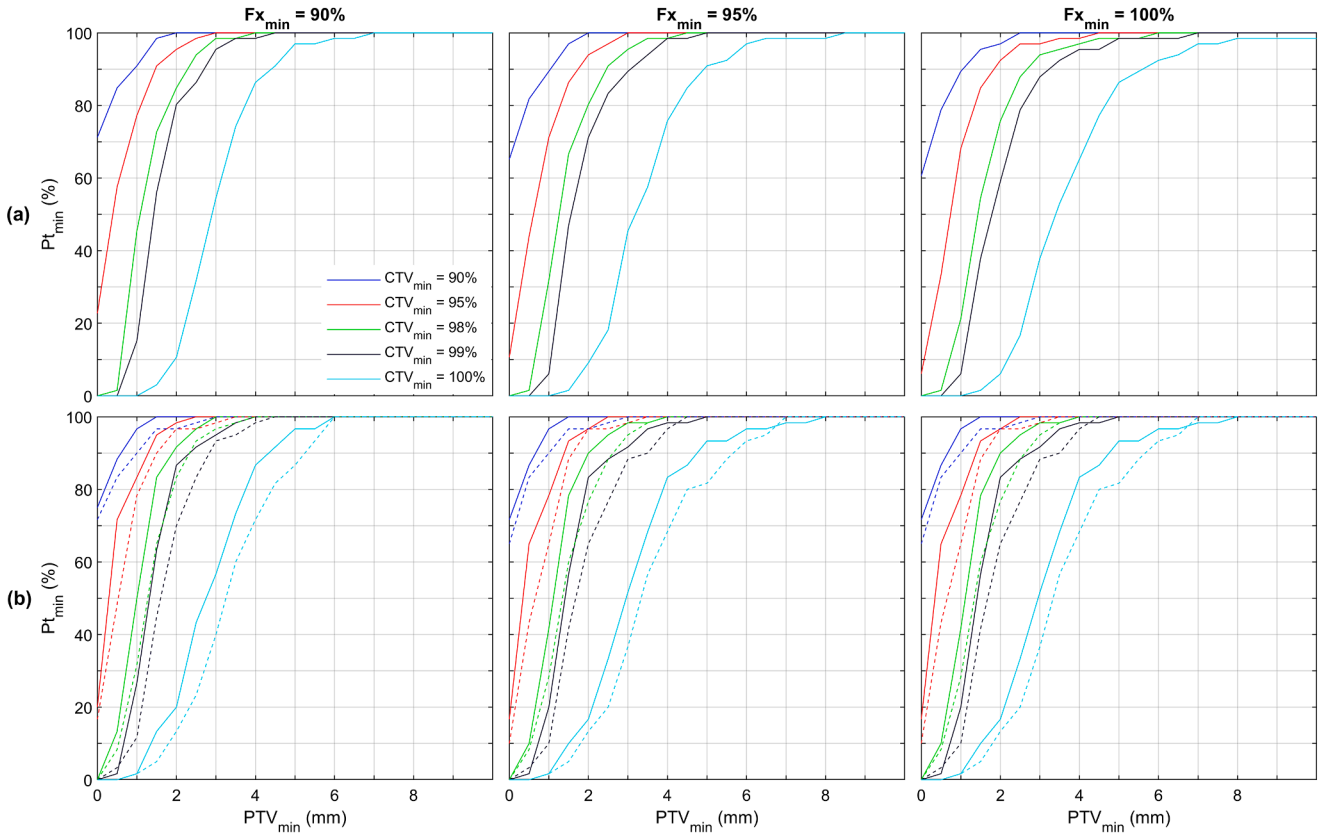

Fig. 3. (a) PTV modeling of target rotational uncertainty. The results show the minimum PTV margin (PTV_{min}; x-axis) to cover ≥ CTV_{min} of the CTV_{fx} volume (individual colored lines) in ≥ Fx_{min} of fractions (individual plots) in ≥ Pt_{min} of patients (y-axis). For example, point A depicts that a 3.0 mm PTV margin is required to cover 98 % of the CTV_{fx} volume in 95 % of fractions in 95 % of patients. Similarly, point B illustrates that a 1.5 mm margin is required to cover 95 % of the CTV_{fx} volume in 90 % of fractions in 90 % of patients. (b) PTV modeling of intrafraction motion. The solid lines denote PTV modeling of residual setup uncertainty for the 60 patient/412 fraction subset with end of fraction repeat T1 imaging. The dashed lines repeat this modeling after the inclusion of intrafraction motion. An additional PTV margin of 0.5 and 0.2 mm (horizontal distance between the solid and dashed lines) is needed to accommodate intrafraction motion for scenarios A and B, respectively.

contouring of both glioma [22] and post-operative metastatic surgical cavities [23] aim to diminish this lingering variability. Ultimately, delineation uncertainty, along with patient setup data and models like those presented here, must be considered in clinical PTV margin designs.

The specific margin recommendations developed in this work are consistent with other PTV margin models and proposals. For example, based on cone-beam computed tomography (CBCT) guided linac stereotactic radiotherapy proposed PTV margins range from 2.0 to 2.8 mm [35,36]. Margin recommendations increase for standard fractionation protocols, with consensus guidelines advocating 3–5 mm for CBCT guided linear accelerator based glioblastoma radiotherapy [37]. Smaller margins are suggested for dedicated radiosurgery systems, ranging from 0.6 mm for single fraction radiosurgery to 1.8 mm for hypofractionated treatments [38,39]. A compelling benefit of the data-driven approach detailed in this work is the direct incorporation of empirical target and OAR contours.

Clinically relevant open questions surround the consequences of different PTV margin strategies. Emerging results for 5-fraction stereotactic radiotherapy for intracranial metastases have identified a 10.0 or 10.5 cm^3 threshold for the normal brain contour excluding the CTV (brain-CTV) receiving 30 Gy as predictive for symptomatic radionecrosis [40,41]. Across the 17 cavity patients included in the current study, the median overlap of the brain-CTV with the PTV was 13.2, 9.9, and 6.4 cm^3 for PTV margins of 4, 3, and 2 mm, respectively, emphasizing the critical importance of a PTV margin strategy to reduce treatment related sequelae. Due to the relative modernity of small volume intracranial primary tumor radiotherapy, similar data on the sensitivity of treatment toxicity and local control to PTV margins are currently not available. Ultimately, improved knowledge on the clinical benefits of these small margin treatments await results from ongoing clinical trials such as those investigating small margin adaptive glioblastoma radiotherapy [10], and stereotactic radiosurgery versus hypofractionated cavity radiotherapy [42].

Driven by the clinical "adapt-to-position" treatment approach [1], an assumption underlying the PTV model developed in this work is that the CTV shape does not change during fractionated radiotherapy. However, recent work has identified meaningful interfraction morphological CTV changes in both the primary tumor [4–7] and post-surgical cavity [8] setting. Of particular note, two studies have identified glioblastoma cohorts in which the maximal linear extent of the GTV and CTV was greater than 2 cm when compared to their planning volumes [6,7]. Recent clinical approaches to glioblastoma radiotherapy mitigate the consequences of such changes either implicitly through reducing the overall length of radiotherapy with a 5-fraction stereotactic protocol [9], or explicitly through weekly online T1 with gadolinium contrast imaging and full plan adaptation with the patient on the MRL couch [10]. An advantage of this latter approach is that interfraction target changes are directly included in the adapted CTV, thereby alleviating the potential need for the PTV to accommodate unobserved morphological target changes. The generality of the PTV model developed in this work allows it to explore the consequences of different PTV margins for such a treatment approach and is a current future direction.

A limitation of the present study is that the CTV coverage was modeled as purely geometric, and the PTV overlap with surrounding

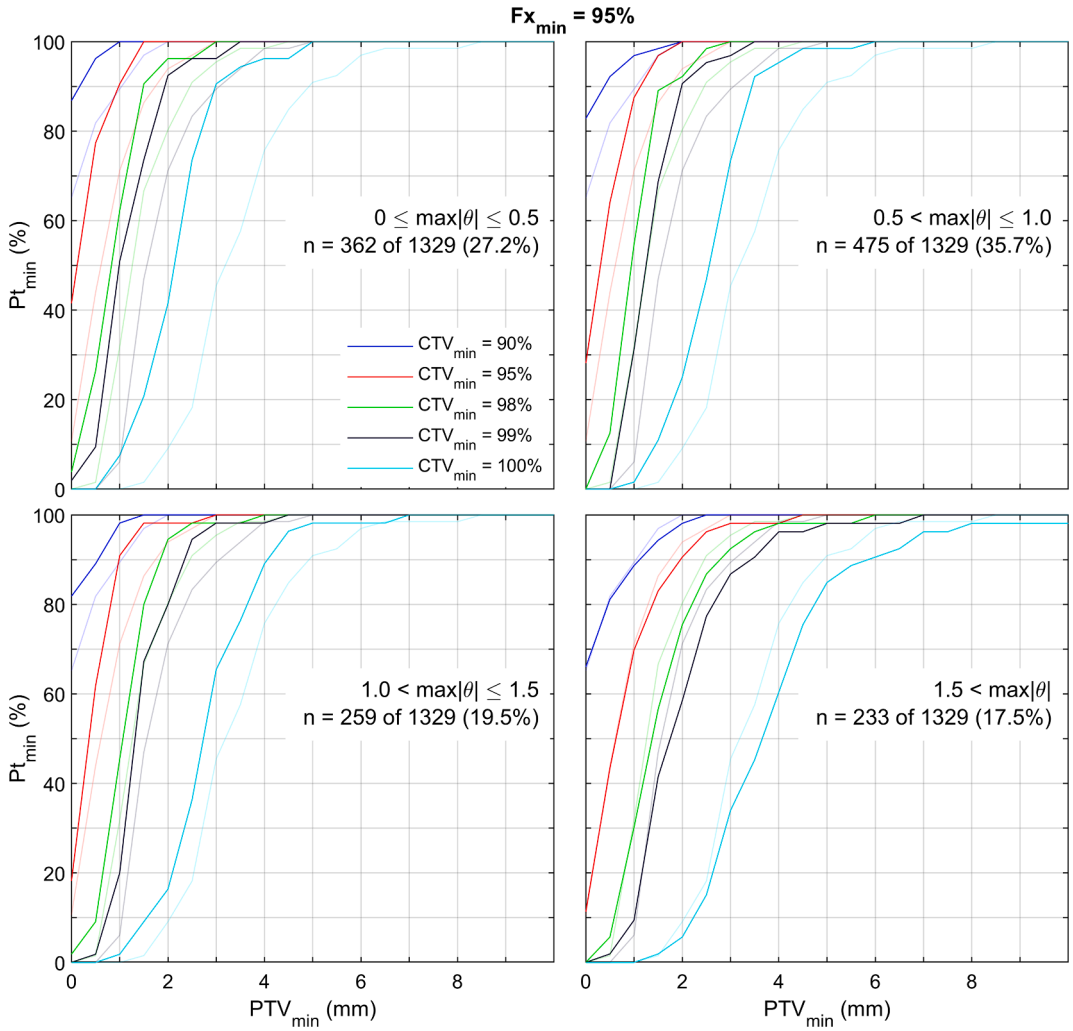

Fig. 4. PTV margin sensitivity to residual rotational target localization uncertainties. Denoting, for each patient fraction, the maximum rotational component across the three patient axes by $\max|\theta|$, the four plots show the PTV model results for the indicated fraction subset in dark lines. The faded lines show the PTV modeling results for all 1329 fractions for reference (i.e. the faded lines in all plots are the same as the middle plot of Fig. 3(a)). Fx_{min} = 95 % for all plots.

OARs and parenchyma was used as a surrogate for the dosimetric consequences of varying PTV margins. CTV coverage, in terms of specific isodoses for the range of PTV margins studied, would lend further support to the clinical relevance of the present study. We have ongoing research involving generating unique treatment plans for each PTV margin (4 mm, 3 mm, 2 mm, etc.) to evaluate the dosimetric impact with respect to CTV coverage. With respect to comparisons with conventional PTV margin design, such as those generated by the van Herk formula [43,44], this was omitted from the present study as such formulae are generally derived from specific radiotherapy techniques and patient populations (e.g. 4-field box treating prostate cancer) that are not directly applicable to the type of plans or technique evaluated here. Furthermore, historical population-based PTV margin designs such as van Herk [43] are often focused on translational setup errors, whereas one of the main sources of uncertainty in the present study arose from rotational setup uncertainties, and often derived analytically with restrictions on the shape of the CTV (for example, assumption of spherical symmetry [43]). In addition, these models are typically more accurate for longer fractionation treatments and are ill-advised for hypofractionated schedules [45]. In contrast, the empirical model developed here does not have a similar restriction and can be applied with equal utility to standard or hypofractionated schedules. Finally, the retrospective six-degree of freedom fusions performed in this study were based on a rigid bony match between the reference CT and the daily MRI. However, in the online setting the co-registration is occasionally manually adjusted off this bony match based on soft-tissue matching, for example in cases where the brain anatomy has changed due to swelling or resolution thereof. The modeling parameters developed in the present study may be somewhat conservative if one accounts for such cases.

Conclusions

We have quantified target localization uncertainty and intrafraction motion for a large series of treated MR-linac brain tumor patients after translation-only MR based patient setup. With these data, we developed a population-based PTV model to explore the consequence of different PTV margins. Based on this model, we recommend a minimum PTV of 2–3 mm for translation-based MR-linac treatments of this indication. This work is a crucial step towards developing an adaptive brain treatment based on dynamic tumor changes and tumor response.

Funding

Department of Radiation Oncology, Sunnybrook Odette Cancer Centre.

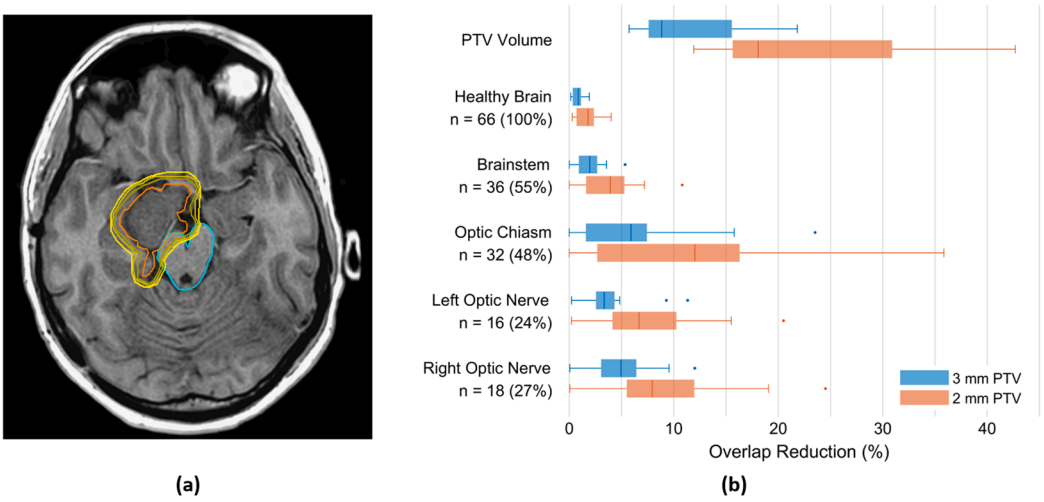

Fig. 5. (a) Illustration of the effect of PTV margin reduction on nearby critical structures in a meningioma patient. Shown on the axial T1 planning MRI are the contours for the CTV (orange), brainstem (cyan), and PTVs, with 2, 3, and 4 mm isotropic margins (increasing brightness in yellow), respectively. In this patient, relative to a 4 mm PTV, margins of 3 and 2 mm reduce the proportion of the brainstem overlapped by the PTV by 5.4 % and 10.8 %, respectively. (b) Quantification of volumetric improvements from PTV margin reduction across all patients. The top group summarizes the reduction in PTV volume relative to a 4 mm PTV; for example, a 2 mm margin reduces the PTV volume by a range of 11.9–42.7 % relative to a 4 mm margin. The other groups describe the reduction in PTV overlap of critical structures. The PTV of 32 patients, for example, overlaps the optic chiasm. Among this patient subgroup, reducing the PTV margin from 4 to 2 mm reduces the proportion of the optic chiasm overlapped by the PTV by a range of 0.0–35.9 %. In all groups, the boxplots delineate the median (vertical line), 25th and 75th percentiles (box edges), most extreme non-outlier values (whiskers), and outliers greater than 150 % of the interquartile range from the box edge (circles). Blue and orange boxplots quantify PTV margin reduction from 4 mm to 3 and 2 mm, respectively. (For interpretation of the references to colour in this figure legend, the reader is referred to the web version of this article.)

Declaration of Competing Interest

The authors declare the following financial interests/personal relationships which may be considered as potential competing interests: *James Stewart*: Employment, Sunnybrook Odette Cancer Centre. *Arjun Sahgal*: Independent Contractor, Sunnybrook Odette Cancer Centre. Grants or contracts: Elekta AB, Varian. Honoraria for lectures and presentations: Varian (medical advisory group & CNS teaching faculty), Elekta (gamma knife ICON), Elekta AB, BrainLab, AstraZeneca, Medtronic Kyphon, Accuray, Merck, Abbvie, Roche. Meeting and travel support: Elekta AB, Varian, BrainLab. Advisory board participation: VieCure. Other: Board member with International Stereotactic Radiosurgery Society (ISRS), co-chair of AO Spine knowledge forum tumor, member of Elekta MR-Linac research consortium, member of Elekta Spine, member of Elekta Oligometastases and Elekta Linac based SRS consortia. *Mahtab M Zadeh*: None. *Bahareh Moazen*: Employment, Sunnybrook Research Institute. *Pejman Jabehdar Maralani*: Independent Contractor, Sunnybrook Health Sciences Centre. *Stephen Breen*: Employment, Sunnybrook Odette Cancer Centre. *Angus Lau*: Employment, Sunnybrook Research Institute. *Shawn Binda*: Employment, Sunnybrook Odette Cancer Centre. *Brain Keller*: Employment, Sunnybrook Odette Cancer Centre. *Zain Husain*: Independent Contractor, Sunnybrook Odette Cancer Centre. *Sten Myrehaug*: Independent Contractor, Sunnybrook Odette Cancer Centre, Grants or contracts: Ipsen Pharmaceuticals, AAA/Novartis, Consulting fees: AAA/Novartis, Honoraria for lectures and presentations: AAA/Novartis. *Jay Detsky*: Independent Contractor, Sunnybrook Odette Cancer Centre. *Hany Soliman:* Independent Contractor, Sunnybrook Odette Cancer Centre. *Chia-Lin Tseng*: Independent Contractor, Sunnybrook Odette Cancer Centre, Honoraria for lectures and presentations: Elekta AB, Meeting and travel support: Elekta AB, Advisory board participation: Sanofi S.A. Leadership on committee: Elekta AB (brain tumor site group lead for MR-Linac consortium). *Mark Ruschin*: Employment, Sunnybrook Odette Cancer Centre, Royalties: Elekta AB, Patents: Image-guided multi-source radiotherapy (US7729473B2).

References

[1] Winkel D, Bol GH, Kroon PS, van Asselen B, Hackett SS, Werensteijn-Honingh AM, et al. Adaptive radiotherapy: The Elekta Unity MR-linac concept. Clin Transl Radiat Oncol 2019;18:54–9. https://doi.org/10.1016/J.CTRO.2019.04.001.
[2] Hall WA, Paulson ES, van der Heide UA, Fuller CD, Raaymakers BW, Lagendijk JJW, et al. The transformation of radiation oncology using real-time magnetic resonance guidance: A review. Eur J Cancer 2019;122:42–52. https://doi.org/10.1016/J.EJCA.2019.07.021.
[3] Cao Y, Tseng C-L, Balter JM, Teng F, Parmar HA, Sahgal A. Mr-guided radiation therapy: Transformative technology and its role in the central nervous system. Neuro Oncol 2017;19(suppl_2):ii16–29. https://doi.org/10.1093/neuonc/nox006.
[4] Manon R, Hui S, Chinnaiyan P, Suh J, Chang E, Timmerman R, et al. The impact of mid-treatment MRI on defining boost volumes in the radiation treatment of glioblastoma multiforme. Technol Cancer Res Treat 2004;3(3):303–7. https://doi.org/10.1177/153303460400300308.
[5] Kim TG, Lim DH. Interfractional variation of radiation target and adaptive radiotherapy for totally resected glioblastoma. J Korean Med Sci 2013;28:1233–7. https://doi.org/10.3346/jkms.2013.28.8.1233.
[6] Stewart J, Sahgal A, Lee Y, Soliman H, Tseng C-L, Detsky J, et al. Quantitating Interfraction Target Dynamics During Concurrent Chemoradiation for Glioblastoma: A Prospective Serial Imaging Study. Int J Radiat Oncol Biol Phys 2021;109(3):736–46. https://doi.org/10.1016/j.ijrobp.2020.10.002.
[7] Bernchou U, Arnold TST, Axelsen B, Klüver-Kristensen M, Mahmood F, Harbo FSG, et al. Evolution of the gross tumour volume extent during radiotherapy for glioblastomas. Radiother Oncol 2021;160:40–6. https://doi.org/10.1016/J.RADONC.2021.04.001.
[8] Tan H, Stewart J, Ruschin M, Wang MH, Myrehaug S, Tseng C-L, et al. Interfraction dynamics during post-operative 5 fraction cavity hypofractionated stereotactic radiotherapy with a MR LINAC: a prospective serial imaging study. J Neurooncol 2022;156(3):569–77. https://doi.org/10.1007/s11060-021-03938-w.
[9] Azoulay M, Chang SD, Gibbs IC, Hancock SL, Pollom EL, Harsh GR, et al. A phase I/II trial of 5-fraction stereotactic radiosurgery with 5-mm margins with concurrent temozolomide in newly diagnosed glioblastoma: Primary outcomes. Neuro Oncol 2020;22(8):1182–9. https://doi.org/10.1093/neuonc/noaa019.
[10] Detsky J (2021) NCT04726397 - UNIty-Based MR-Linac Guided AdapTive RadiothErapy for High GraDe Glioma: A Phase 2 Trial (UNITED). In: ClinicalTrials.gov.
[11] Soliman H, Myrehaug S, Tseng C-L, Ruschin M, Hashmi A, Mainprize T, et al. Image-Guided, Linac-Based, Surgical Cavity-Hypofractionated Stereotactic Radiotherapy in 5 Daily Fractions for Brain Metastases. Clin Neurosurg 2019;85(5):E860–9.
[12] Eaton BR, La Riviere MJ, Kim S, Prabhu RS, Patel K, Kandula S, et al. (2015) Hypofractionated radiosurgery has a better safety profile than single fraction radiosurgery for large resected brain metastases. J Neuro-Oncol 2015;123(1):103–11.

[13] Abuodeh Y, Ahmed KA, Naghavi AO, Venkat PS, Sarangkasiri S, Johnstone PAS, et al. Postoperative Stereotactic Radiosurgery Using 5-Gy × 5 Sessions in the Management of Brain Metastases. World Neurosurg 2016;90:58–65. https://doi.org/10.1016/J.WNEU.2016.02.007.
[14] Minniti G, Esposito V, Clarke E, Scaringi C, Lanzetta G, Salvati M, et al. Multidose Stereotactic Radiosurgery (9 Gy × 3) of the Postoperative Resection Cavity for Treatment of Large Brain Metastases. Int J Radiat Oncol 2013;86(4):623–9. https://doi.org/10.1016/J.IJROBP.2013.03.037.
[15] Keller A, Doré M, Cebula H, Thillays F, Proust F, Darié I, et al. Hypofractionated Stereotactic Radiation Therapy to the Resection Bed for Intracranial Metastases. Int J Radiat Oncol 2017;99(5):1179–89. https://doi.org/10.1016/J.IJROBP.2017.08.014.
[16] Lima LCS, Sharim J, Levin-Epstein R, Tenn S, Teles AR, Kaprealian T, et al. Hypofractionated Stereotactic Radiosurgery and Radiotherapy to Large Resection Cavity of Metastatic Brain Tumors. World Neurosurg 2017;97:571–9. https://doi.org/10.1016/J.WNEU.2016.10.076.
[17] Lockney NA, Wang DG, Gutin PH, et al. Clinical outcomes of patients with limited brain metastases treated with hypofractionated (5 × 6 Gy) conformal radiotherapy. Radiother Oncol 2017;123:203–8. https://doi.org/10.1016/J.RADONC.2017.03.018.
[18] Eitz KA, Lo SS, Soliman H, Sahgal A, Theriault A, Pinkham MB, et al. Multi-institutional Analysis of Prognostic Factors and Outcomes after Hypofractionated Stereotactic Radiotherapy to the Resection Cavity in Patients with Brain Metastases. JAMA Oncol 2020;6(12):1901.
[19] Bol GH, Lagendijk JJW, Raaymakers BW. Virtual couch shift (VCS): accounting for patient translation and rotation by online IMRT re-optimization. Phys Med Biol 2013;58(9):2989. https://doi.org/10.1088/0031-9155/58/9/2989.
[20] Ruschin M, Sahgal A, Tseng C-L, Sonier M, Keller B, Lee Y. Dosimetric Impact of Using a Virtual Couch Shift for Online Correction of Setup Errors for Brain Patients on an Integrated High-Field Magnetic Resonance Imaging Linear Accelerator. Int J Radiat Oncol 2017;98(3):699–708. https://doi.org/10.1016/J.IJROBP.2017.03.004.
[21] Tseng C-L, Chen H, Stewart J, et al. High grade glioma radiation therapy on a high field 1.5 Tesla MR-Linac: Workflow and initial experience with daily adapt-to-position (ATP) MR guidance: A first report. Front. Oncol 2022;12(1060098). https://doi.org/10.3389/fonc.2022.1060098.
[22] Tseng C-L, Stewart J, Whitfield G, Verhoeff JJC, Bovi J, Soliman H, et al. Glioma consensus contouring recommendations from a MR-Linac International Consortium Research Group and evaluation of a CT-MRI and MRI-only workflow. J Neurooncol 2020;149(2):305–14. https://doi.org/10.1007/s11060-020-03605-6.
[23] Soliman H, Ruschin M, Angelov L, Brown PD, Chiang VLS, Kirkpatrick JP, et al. Consensus Contouring Guidelines for Postoperative Completely Resected Cavity Stereotactic Radiosurgery for Brain Metastases. Int J Radiat Oncol Biol Phys 2018;100(2):436–42. https://doi.org/10.1016/J.IJROBP.2017.09.047.
[24] Jhaveri J, Chowdhary M, Zhang X, Press RH, Switchenko JM, Ferris MJ, et al. Does size matter? Investigating the optimal planning target volume margin for postoperative stereotactic radiosurgery to resected brain metastases. J Neurosurg 2019;130(3):797–803. https://doi.org/10.3171/2017.9.JNS171735.
[25] Lanberg T, Chavaudra J, Dobbs J, et al (2016) ICRU Report 50.
[26] Weygand J, Fuller CD, Ibbott GS, et al. Spatial precision in magnetic resonance imaging-guided radiation therapy: The role of geometric distortion. Int J Radiat Oncol Biol Phys 2016;95:1304–16.
[27] Emmerich J, Laun FB, Pfaffenberger A, Schilling R, Denoix M, Maier F, et al. Technical Note: On the size of susceptibility-induced MR image distortions in prostate and cervix in the context of MR-guided radiation therapy. Med Phys 2018;45(4):1586–93. https://doi.org/10.1002/mp.12785.
[28] Hood MN, Ho VB, Smirniotopoulos JG, Szumowski J. Chemical shift: The artifact and clinical tool revisited. Radiographics 1999;19:357–71. https://doi.org/10.1148/radiographics.19.2.g99mr07357.
[29] Dorsch S, Mann P, Elter A, Runz A, Spindeldreier CK, Klüter S, et al. Measurement of isocenter alignment accuracy and image distortion of an 0.35 T MR-Linac system. Phys Med Biol 2019;64(20):205011.
[30] Tijssen RHN, Philippens MEP, Paulson ES, Glitzner M, Chugh B, Wetscherek A, et al. MRI commissioning of 1.5T MR-linac systems – a multi-institutional study. Radiother Oncol 2019;132:114–20. https://doi.org/10.1016/j.radonc.2018.12.011.
[31] Bernchou U, Christiansen RL, Bertelsen A, Tilly D, Riis HL, Jensen HR, et al. End-to-end validation of the geometric dose delivery performance of MR linac adaptive radiotherapy. Phys Med Biol 2021;66(4). https://doi.org/10.1088/1361-6560/abd3ed. 045034.
[32] Weltens C, Menten J, Feron M, Bellon E, Demaerel P, Maes F, et al. Interobserver variations in gross tumor volume delineation of brain tumors on computed tomography and impact of magnetic resonance imaging. Radiother Oncol 2001;60(1):49–59. https://doi.org/10.1016/S0167-8140(01)00371-1.
[33] Cattaneo GM, Reni M, Rizzo G, Castellone P, Ceresoli GL, Cozzarini C, et al. Target delineation in post-operative radiotherapy of brain gliomas: Interobserver variability and impact of image registration of MR(pre-operative) images on treatment planning CT scans. Radiother Oncol 2005;75(2):217–23. https://doi.org/10.1016/j.radonc.2005.03.012.
[34] Wee CW, Sung W, Kang H-C, Cho KH, Han TJ, Jeong B-K, et al. Evaluation of variability in target volume delineation for newly diagnosed glioblastoma: A multi-institutional study from the Korean Radiation Oncology Group. Radiat Oncol 2016;10(1). https://doi.org/10.1186/s13014-015-0439-z.
[35] Seravalli E, Van Haaren PMA, Van Der Toorn PP, Hurkmans CW. A comprehensive evaluation of treatment accuracy, including end-to-end tests and clinical data, applied to intracranial stereotactic radiotherapy. Radiother Oncol 2015;116:131–8. https://doi.org/10.1016/J.RADONC.2015.06.004.
[36] Naoi Y, Kunishima N, Yamamoto K, Yoda K. A planning target volume margin formula for hypofractionated intracranial stereotactic radiotherapy under cone beam CT image guidance with a six-degrees-offreedom robotic couch and a mouthpiece-assisted mask system: A preliminary study. Br J Radiol 2014;87. https://doi.org/10.1259/BJR.20140240/FORMAT/EPUB.
[37] Niyazi M, Brada M, Chalmers AJ, Combs SE, Erridge SC, Fiorentino A, et al. ESTRO-ACROP guideline "target delineation of glioblastomas". Radiother Oncol 2016;118(1):35–42. https://doi.org/10.1016/j.radonc.2015.12.003.
[38] Li WTY. Determining Rational Planning Target Volume Margins for Intracranial Stereotactic Radiotherapy. University of Toronto; 2014.
[39] MacDonald RL, Lee Y, Schasfoort J, Soliman H, Sahgal A, Ruschin M. Real-Time Infrared Motion Tracking Analysis for Patients Treated With Gated Frameless Image Guided Stereotactic Radiosurgery. Int J Radiat Oncol Biol Phys 2020;106(2):413–21. https://doi.org/10.1016/j.ijrobp.2019.10.030.
[40] Faruqi S, Ruschin M, Soliman H, Myrehaug S, Zeng KL, Husain Z, et al. Adverse Radiation Effect After Hypofractionated Stereotactic Radiosurgery in 5 Daily Fractions for Surgical Cavities and Intact Brain Metastases. Int J Radiat Oncol Biol Phys 2020;106(4):772–9. https://doi.org/10.1016/J.IJROBP.2019.12.002.
[41] Andruska N, Kennedy WR, Bonestroo L, Anderson R, Huang Yi, Robinson CG, et al. Dosimetric predictors of symptomatic radiation necrosis after five-fraction radiosurgery for brain metastases. Radiother Oncol 2021;156:181–7. https://doi.org/10.1016/J.RADONC.2020.12.011.
[42] Single Fraction Stereotactic Radiosurgery Compared With Fractionated Stereotactic Radiosurgery in Treating Patients With Resected Metastatic Brain Disease - Full Text View - ClinicalTrials.gov. https://clinicaltrials.gov/ct2/show/NCT04114981. Accessed 25 Mar 2022.
[43] Van Herk M, Remeijer P, Rasch C, Lebesque JV. The probability of correct target dosage: Dose-population histograms for deriving treatment margins in radiotherapy. Int J Radiat Oncol Biol Phys 2000;47:1121–35. https://doi.org/10.1016/S0360-3016(00)00518-6.
[44] Van Herk M. Errors and Margins in Radiotherapy. Semin Radiat Oncol 2004;14:52–64. https://doi.org/10.1053/j.semradonc.2003.10.003.
[45] Herschtal A, Foroudi F, Silva L, Gill S, Kron T. Calculating geometrical margins for hypofractionated radiotherapy. Phys Med Biol 2012;58(2):319. https://doi.org/10.1088/0031-9155/58/2/319.